Journal of Applied Physics

Unification of the negative electrocaloric effect in $Bi_{1/2}Na_{1/2}TiO_3$-$BaTiO_3$ solid solutions by $Ba_{1/2}Sr_{1/2}TiO_3$ doping

Cite as: J. Appl. Phys. **114**, 213519 (2013); https://doi.org/10.1063/1.4842935
Submitted: 10 October 2013 . Accepted: 22 November 2013 . Published Online: 06 December 2013

Sarir Uddin, Guang-Ping Zheng, Yaseen Iqbal, Rick Ubic, and Junhe Yang

Unification of the negative electrocaloric effect in $Bi_{1/2}Na_{1/2}TiO_3$-$BaTiO_3$ solid solutions by $Ba_{1/2}Sr_{1/2}TiO_3$ doping

Sarir Uddin,[1,2] Guang-Ping Zheng,[1,3,a)] Yaseen Iqbal,[2] Rick Ubic,[4] and Junhe Yang[3]
[1]*Department of Mechanical Engineering, The Hong Kong Polytechnic University, Hung Hom, Kowloon, Hong Kong*
[2]*Materials Research Laboratory, Institute of Physics and Electronics, University of Peshawar, Peshawar 25120, Pakistan*
[3]*School of Materials Science and Engineering, The University of Shanghai for Science and Technology, Shanghai, China*
[4]*Department of Materials Science and Engineering, Boise State University, Boise, Idaho 83725-2090, USA*

(Received 10 October 2013; accepted 22 November 2013; published online 6 December 2013)

The microscopic mechanisms of the negative electrocaloric effect (ECE) of the single-phase $(1-x)(0.94Bi_{1/2}Na_{1/2}TiO_3\text{-}0.06BaTiO_3)\text{-}xBa_{1/2}Sr_{1/2}TiO_3$ (BNT-BT-BST) perovskite solid solutions fabricated via the sol-gel technique are explored in this study. Dielectric and mechanical relaxation analyses are employed to investigate the ferroelectric and structural transitions of the samples. The electrocaloric properties of the samples were measured by thermodynamics Maxwell relations. The difference between the depolarization temperature (T_d) and the maximum dielectric constant temperature (T_m) was found to decrease with increasing BST content. Doping with BST stabilized the ferroelectric phase along with unifying the EC temperature changes (ΔT) to only negative values. The origin of the uniform negative ECE of BNT-BT-BST is discussed. © *2013 AIP Publishing LLC*. [http://dx.doi.org/10.1063/1.4842935]

I. INTRODUCTION

The adiabatic temperature change of a polarizable material caused by an applied electric field is termed as the electrocaloric effect (ECE) and was discovered in crystalline Rochelle salt ($KNaC_4H_4O_6{\cdot}4H_2O$) by Kobeko *et al.*[1] The ECE can be potentially utilized in designing solid-state environmental-friendly cooling systems at small scales for electronic devices, to replace fan-based cooling systems. A solid-state ECE refrigerator can be designed as one in which the temperature of the solid-state working material is decreased due to the application or withdrawal (depending on whether the ECE of the materials in questions is positive or negative) of an applied electric field while in contact with the thermal load. The cooled working material absorbs heat from the thermal load. When the temperature of the working material is increased, it is isolated from the thermal load and the heat is rejected to a sink, and the process is repeated. For materials with positive ECE, the cooling is produced during the withdrawal of the electric field while for negative ECE the cooling effect is produced by increasing the applied electric field.[2] In order to design a practical and usable electrocaloric refrigerator, materials with strong ECE are needed.

A number of materials exhibiting a positive ECE have been reported.[3–10] On the other hand, Bai *et al.*[2] reported the observation of a negative ECE for the first time in $Bi_{1/2}Na_{1/2}TiO_3$-$BaTiO_3$ solid solution at temperature ranging from 25 to 145 °C. Zheng *et al.*[8] have observed the coexistence of a positive and negative ECE as well as the reversal of the sign of ECE above 160 °C in the morphotropic-phase-boundary (MPB) composition $0.94(Bi_{1/2}Na_{1/2}TiO_3)\text{-}0.06BaTiO_3$ (0.94BNT-0.06BT) which can adversely affect the operation of a cooling system at high temperatures. A similar coexistence of a positive and negative ECE was also observed via both direct and indirect measurement techniques by Goupil *et al.*[11] in the $Pb_{1/3}Mg_{2/3}O_3\text{-}30PbTiO_3$ single crystals. The simulation of the ECE for a single crystal of $Ba_{0.5}Sr_{0.5}TiO_3$ also revealed the coexistence of both a positive and negative ECE.[12] Axelsson *et al.*[13] used a statistical mechanics model to deduce and explain the negative ECE in $PbMg_{1/3}Nb_{2/3}O_3\text{-}30PbTiO_3$ (PMN-PT) single crystal.

For the smooth and uniform function of a simple electrocaloric (EC) cooling device, a uniform ECE is necessary rather than the coexistence of both positive and negative ECE. Since 0.94BNT-0.06BT has a relatively large pyroelectric coefficient ($\partial P/\partial T$), it can potentially be used as EC refrigerant in the EC refrigerators; however, one of the drawbacks of this material is the coexistence of both a negative and positive ECE. The cause of this dual nature of the ECE in the same material at different temperatures may be the transition as reported by Axelsson *et al.*[13] In order to stabilize either form of the ECE in the 0.94BNT-0.06BT ceramics the relevant phase transitions must be unified to one phase transition or the transition temperature difference between the ferroelectric-to-antiferroelectric (FE-to-AFE) and antiferroelectric-to-paraelectric (AFE-to-PE) phase transitions must be decreased via specific doping; consequently, the phase transition behaviors of 0.94BNT-0.06BT ceramics with different doping have been investigated in previous studies.[14–17]

In this work, $Ba_{1/2}Sr_{1/2}TiO_3$ (BST) has been used as a probe to investigate the cause of the coexistence of ECE

a)E-mail: mmzheng@polyu.edu.hk

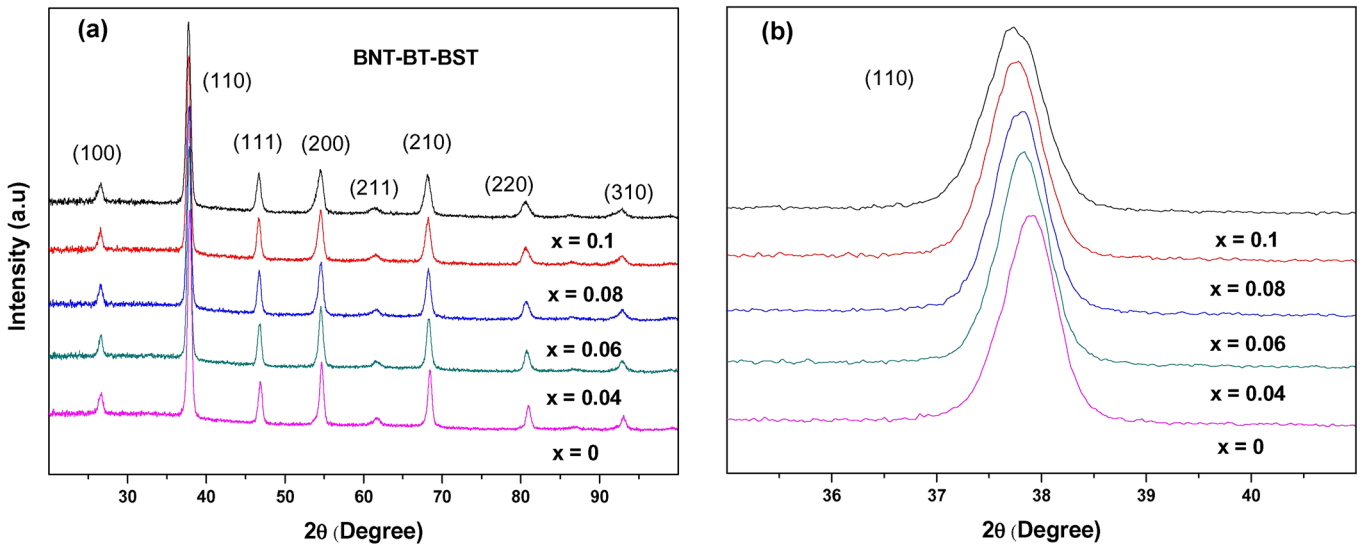

FIG. 1. (a) XRD patterns of BNT-BT-BST samples. (b) Shifting of the (110) peak towards relatively lower 2θ value.

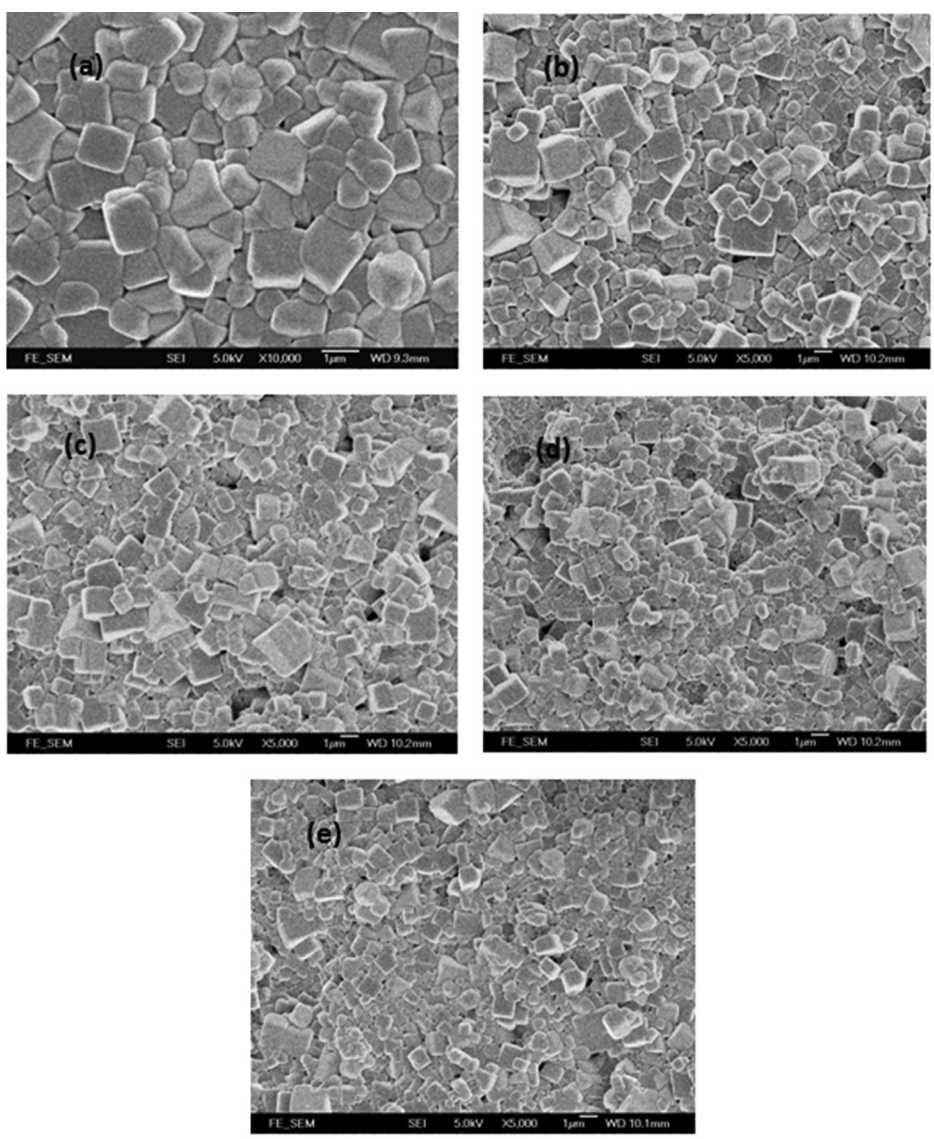

FIG. 2. Secondary electron SEM micrographs of the BNT-BT-BST ceramics sintered at 1100 °C for 2 h in ambient atmosphere: (a) x = 0, (b) x = 0.04, (c) x = 0.06, (d) x = 0.08, and (e) x = 0.1.

with opposite signs and to look for a possible way to unify the ECE as either positive or negative type. Dielectric and mechanical relaxation analyses are employed to elucidate the effect of BST doping on the structural and EC properties of BNT-BT-BST.

II. EXPERIMENTAL DETAILS

Ceramics in the composition series $(1-x)(0.94Bi_{1/2}Na_{1/2}TiO_3\text{-}0.06BaTiO_3)\text{-}xBa_{1/2}Sr_{1/2}TiO_3$ (BNT-BT-BST), with $x = 0$, 0.04, 0.06, 0.08, and 0.1 were fabricated via sol-gel processing method. Solutions of bismuth acetate ($Bi(CH_3COO)_3$) (>99.99% Aldrich), sodium acetate ($Na(CH_3COO)$) (>99% reagent grade Sigma-Aldrich), barium acetate ($Ba(CH_3COO)_2$) (>99% reagent ACS Sigma-Aldrich), and strontium acetate ($Sr(CH_3COO)_2$) (>99% reagent ACS Sigma-Aldrich) in stoichiometric ratios were separately prepared in acetic acid on a hot plate and stirred with a magnetic stirrer. The solution of titanium(IV) butoxide ($C_{16}H_{36}O_4Ti$) (99% reagent grade Aldrich) was prepared in ethanol to which acetylacetone was added drop-wise in order to stabilize the solution. A yellowish colored stable solution was obtained by mixing these five solutions in an Erlenmeyer flask on a hot plate.

A yellowish colored gel was obtained by stirring the stock solution on a hot plate at 100 °C for 4 h. The gel was dried on a hot plate at 100 °C and calcined at 800 °C for 2 h. The calcined powders were pressed into disks of 15 mm diameter for ferroelectric measurements via uni-axial pressing at 300. For mechanical relaxation analysis, 20 × 7 × 1 cm samples were prepared. The samples were finally sintered in air at 1100 °C.

The phase and microstructure analyses were carried out on an X-ray diffractometer (XRD, Bruker D8 advance) and a field emission scanning electron microscope (SEM, JEOL JSM-6335F), respectively. In order to measure dielectric and ferroelectric properties, silver paste was coated to the top and bottom faces of the pellets and heat treated at 700 °C for 20 min. The temperature-dependent relative permittivity (ε_r) and loss tangent ($\tan\delta$) of ceramics were measured at different frequencies using an impedance analyzer (HP 4192A). The anelastic properties of the ceramics were investigated by a dynamic mechanical analyzer (DMA, TA Instruments Q800). The temperature-dependent polarization data were obtained at a frequency of 10 Hz using a ferroelectric test system (TF Analyzer 2000E, aixACCT Systems) every 10 °C temperature interval.

III. RESULTS AND DISCUSSIONS

Figures 1(a) and 1(b) show the room-temperature XRD patterns of the ceramics which revealed the formation of a

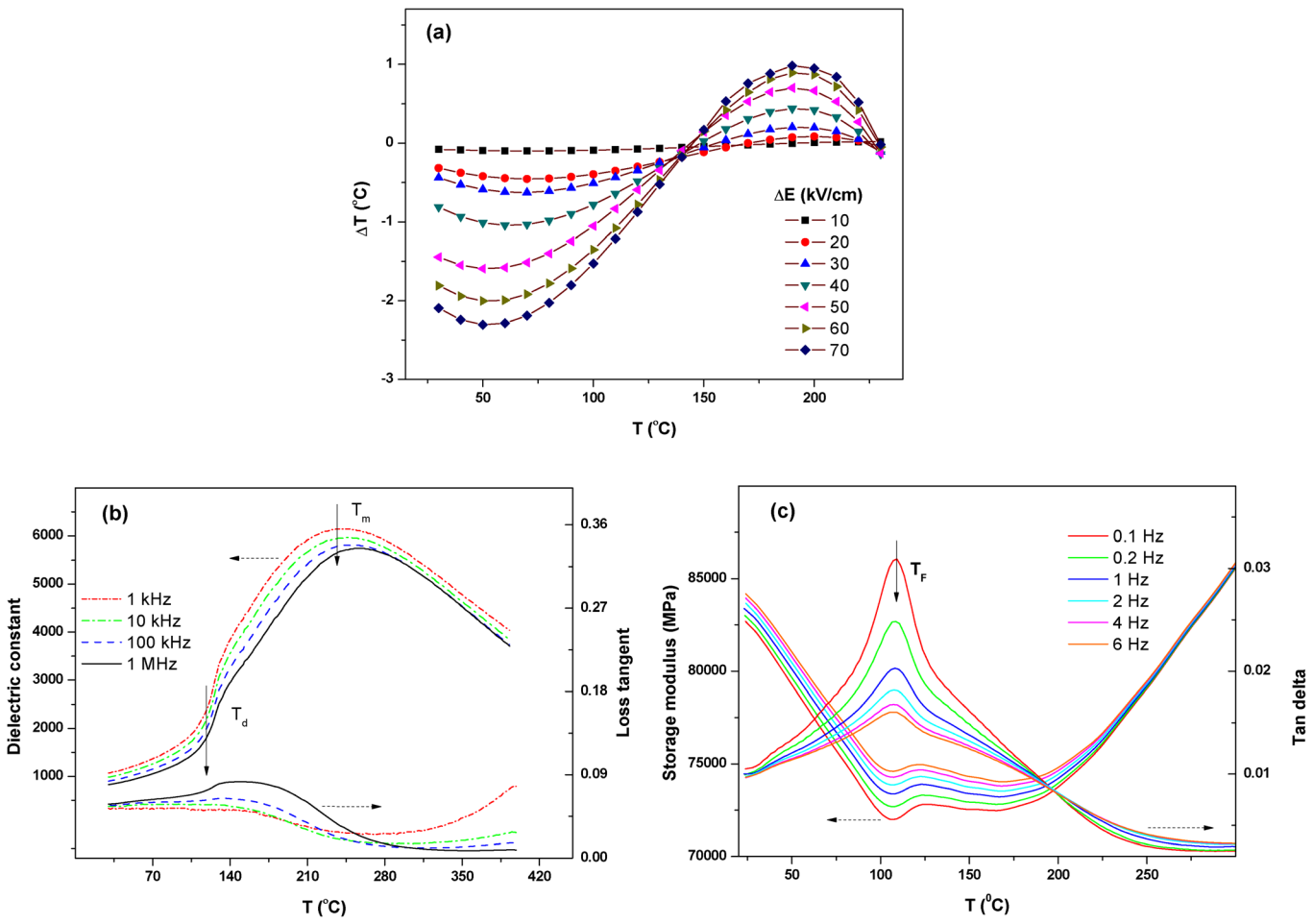

FIG. 3. (a) Electric field and temperature dependences of the electrocaloric temperature changes (ΔT), (b) temperature dependent dielectric constant (ε_r) and loss tangent ($\tan\delta$), and (c) temperature dependence of storage modulus and mechanical loss of 0.94BNT-0.06BT ceramics.

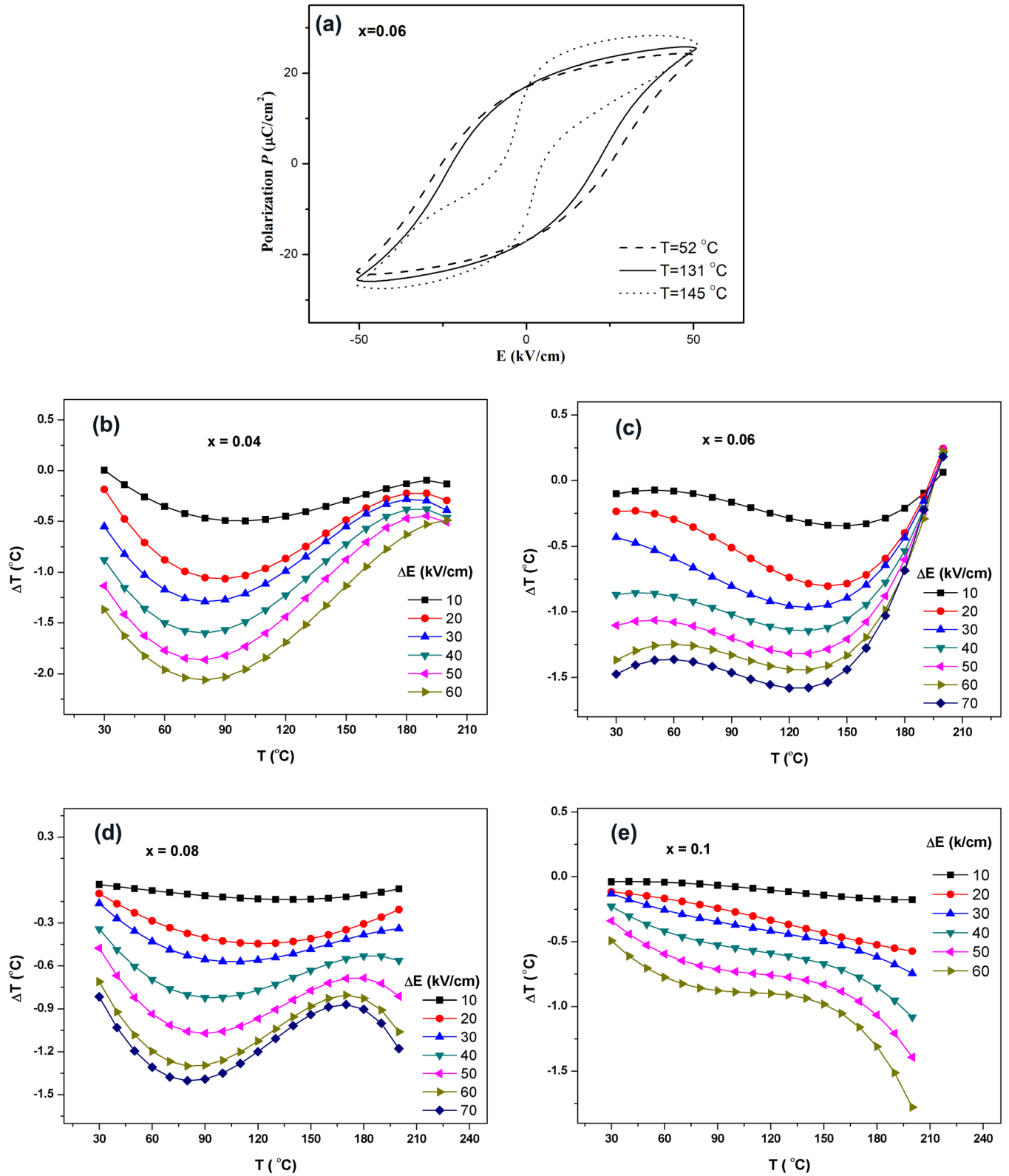

FIG. 4. (a) Typical P-E hysteresis loops of BNT-BT-BST at various temperatures. The content of BST is x = 0.06. (b)-(e) Electric field and temperature dependences of the electrocaloric temperature changes (ΔT) of BNT-BT-BST ceramics: (b) x = 0.04, (c) x = 0.06, (d) x = 0.08, and (e) x = 0.1.

single-phase perovskite structure with no impurity within the detection limit. It was observed that the XRD peaks shifted to lower 2θ values with increasing BST content, as shown in Fig. 1(b), which could be attributed to the substitutions of the relatively larger Ba^{2+}/Sr^{2+} ($R_{Ba}/R_{Sr} = 1.61/1.44$ Å) ions on the A site of the perovskite structure, replacing Bi^{3+}/Na^{+} ($R_{Bi}/R_{Na} = 1.40/1.39$ Å) ions.[18] SEM of the fractured surface of the sintered ceramics (Fig. 2) revealed dense microstructure with nearly uniform grain size and a slight decrease was observed in the grain size with increasing BST content.

The adiabatic temperature changes (ΔT) of the fabricated samples were calculated using a Maxwell relation as follows:

$$\Delta T = -\frac{1}{\rho}\int_{E_1}^{E_2}\frac{T}{C}\left(\frac{\partial P}{\partial T}\right)_E dE. \quad (1)$$

Here, ρ is the mass density, T is the ambient temperature, and c is the specific heat capacity which is assumed to be temperature independent. The values of $(\partial P/\partial T)_E$ were calculated from a fourth-order polynomial fit of the P_{max} vs. T data, where P_{max} is the saturation polarization. $\Delta E = E_2 - E_1$ is the range of the applied electric field.

The EC properties of the fabricated 0.94BNT-0.06BT samples are shown in Fig. 3(a), which indicates the coexistence of negative and positive ECE at 30–230 °C close to the FE-to-AFE and AFE-to-PE phase transition temperatures, respectively. The FE-to-AFE and AFE-to-PE ferroelectric and structural transitions were investigated by the temperature-dependent dielectric properties and dynamic mechanical analysis as shown in Figs. 3(b) and 3(c), respectively. The observed negative ECE below the FE-to-AFE phase transition is a consequence of the increase in polarization with temperature where $(\partial P/\partial T)_E$ has positive values and negative ΔT values can be obtained from the macroscopic thermodynamics relations (Eq. (1)). In the microscopic perspective, the negative ECE could be caused by the changes of parallel dipoles in the FE domains into antiparallel dipoles under the applied electric field and even below the FE-to-AFE transition temperature, which results in the field-driven formation of nano-sized AFE domain walls. According to the formation mechanisms of the AFE incommensurate phase,[19,20] the twinning planes in the modulated AFE state are formed by the re-orientation of the oxygen octahedra in the rhombohedral FE phase, resulting in the formation of the nonpolar tetragonal AFE phase. The applied electric field facilitates such re-orientation by driving the migration of oxygen ions and vacancies; therefore, the application of an electric field either favors the formation of the AFE state or increases dipolar disorder (i.e., entropy), resulting in a negative ECE. The mechanisms of the negative ECE in 0.94BNT-0.06BT are consistent with those suggested by Ponomareva and Lisenkov[12] who attributed the negative ECE to the noncollinearity of the applied electric field and the polarization directions of the pre-poled single crystal sample.

Axelsson *et al.*[13] used the statistical mechanics model to determine the EC properties of single-crystal PMN-PT. They observed the coexistence of positive and negative ECE at a relatively low electric field of 10 kV/cm. According to their microscopic model, the coexistence of a dual nature ECE requires two phase transitions very close in temperature.

Fig. 4(a) shows typical P-E loops of the BNT-BT-BST solid solutions. The effects of BST doping on the EC properties of BNT-BT-BST are shown in Figs. 4(b)–4(e). The values of the EC temperature changes (ΔT) were unified to negative values by the BST doping in the present study, as shown in Fig. 4. The relation between |ΔT| and the BST doping x is shown in Fig. 5(b). Although absolute values of |ΔT| determined from Eq. (1) cannot describe exactly the ECE of BNT-BT-BST solid solutions because of the nonergodic

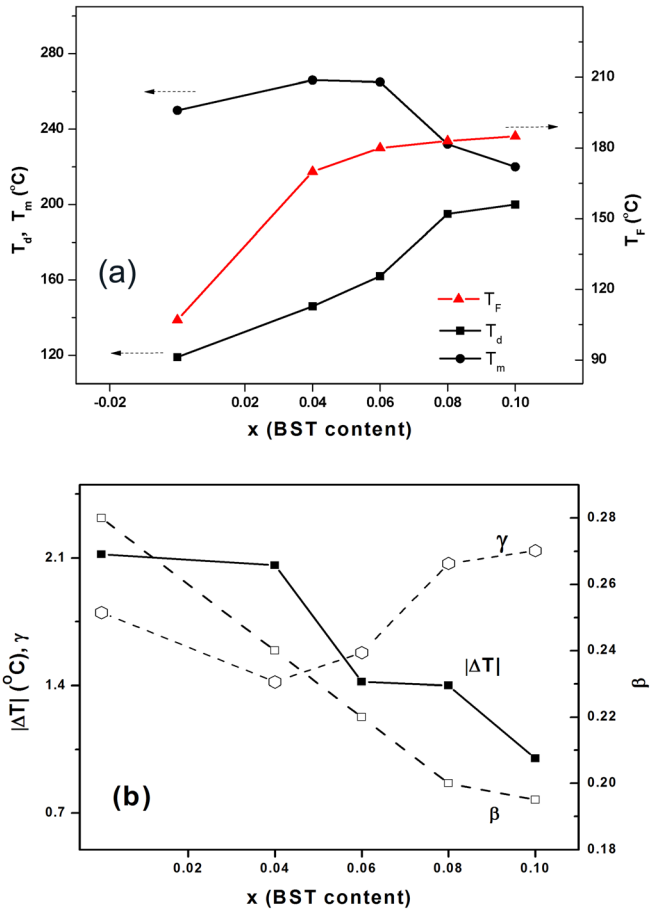

FIG. 5. (a) Dependences of depolarization temperature (T_d), maximum dielectric constant temperature (T_m), and structural T_F on BST content of the BNT-BT-BST samples. (b) Dependence of absolute values of ECE temperature changes on BST content x at 80 °C, and the relations between the exponents β and γ, and the BST content x.

nature of the FE-to-PE or AFE-to-PE transition, the results shown in Fig. 4 reveal meaningful characteristics of ECE in these systems.

BST is a ferroelectric ceramic possessing a high dielectric constant and relatively low Curie temperature (T_c) which is a function of Ba^{2+}/Sr^{2+} ratio. The FE-to-PE phase transition temperature of $Ba_{1/2}Sr_{1/2}TiO_3$ is −1 °C. 0.94BNT-0.06BT has an FE-to-AFE transition at about 122 °C and an AFE-to-PE phase at 250 °C; and the BST doping may affect these phase transitions. Since the electrocaloric properties of the ferroelectrics were affected by their phase transition behaviors, the effects of BST doping on the ferroelectric and structural transitions of BNT-BT-BST were investigated in order to further reveal the microscopic mechanisms of the uniform ECE in BNT-BT-BST.

The effects of BST doping on the phase transitions of BNT-BT-BST were first investigated via dielectric analysis. The plots of the dielectric constant (ε_r) and loss tangent ($\tan\delta$) versus temperature at various frequencies are shown in Fig. 6 and reveal the phase transition behavior of the BNT-BT-BST samples. Doping with BST effectively changed the phase transition temperatures of 0.94BNT-0.06BT ceramics. Two anomalies were observed on ε_r versus T curves at temperatures denoted by T_d and T_m corresponding to the depolarization and

maximum dielectric constant temperature, respectively. It was observed that the difference between these two phase transition temperatures decreased with increasing BST content which could affect the ECE of the BNT-BT-BST ceramics. As shown in Fig. 5(a), the values of the T_m decreased while those of T_d increased with increasing BST content, the effect of which was the stabilization of the ferroelectric phase at higher temperatures. This phenomenon could be caused by the substitution of Ba^{2+}/Sr^{2+} ions for Na^{+} cations on the A site, which could stabilize the oxygen octahedra and the transition from the FE state to the AFE state occurs at higher T_d. The simultaneous reduction in T_m could be caused by the increasing diffuseness of the AFE-to-PE transition due to the Ba^{2+}/Sr^{2+} doping.

As shown in Fig. 6, the curves for temperature-dependent dielectric constant close to the AFE-to-PE transition revealed stronger frequency dispersion for larger BST content, which indicated stronger relaxor behavior of these samples[21] compared with that of 0.94BNT-0.06BT (Fig. 3(b)) when the BST content is larger than 0.06. Close to the AFE-to-PE transition temperature, the applied electric field does not favor the AFE state not only because the oxygen octahedra have been stabilized by the BST doping but also because the electric field

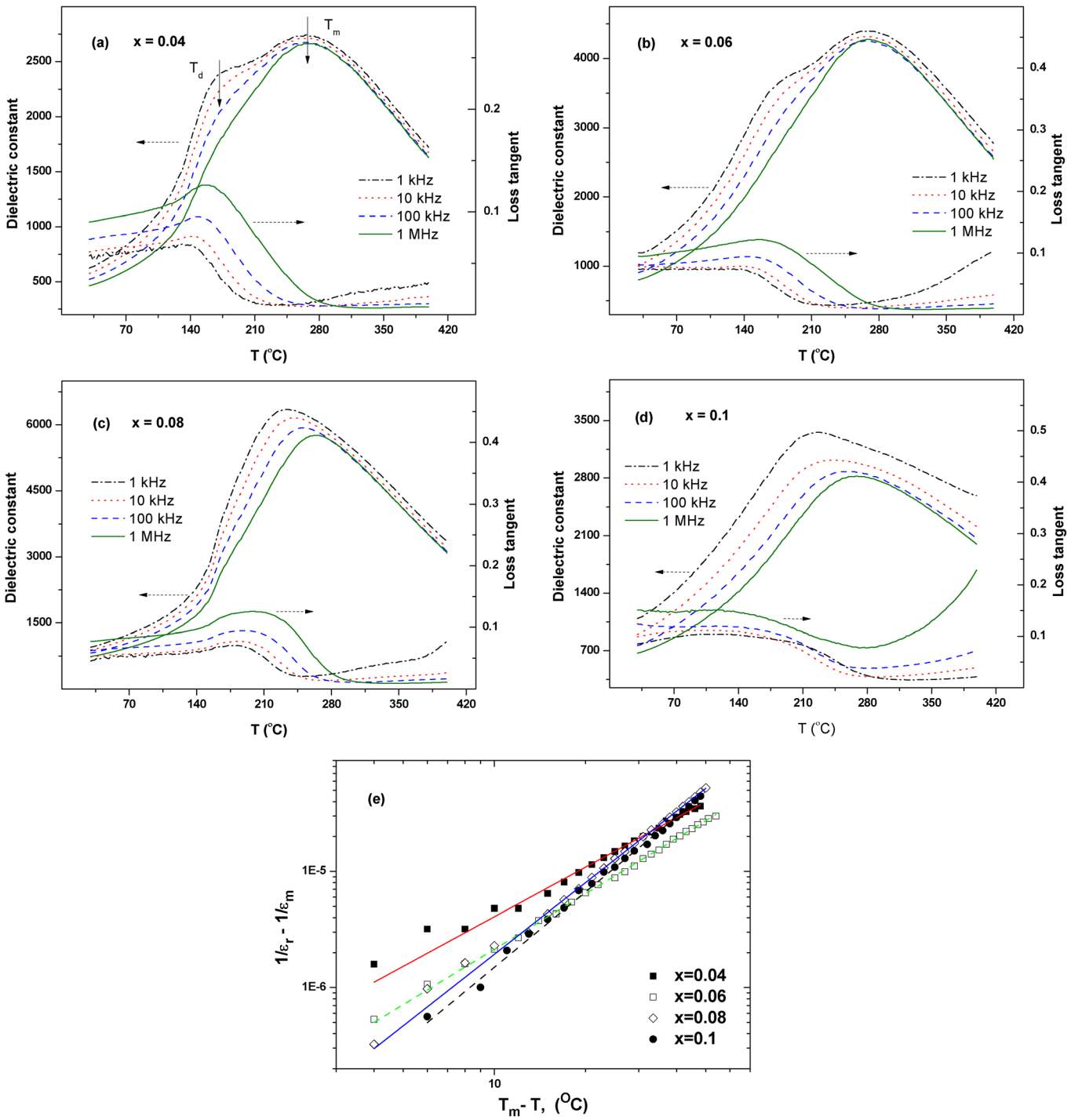

FIG. 6. Temperature and frequency dependences of dielectric constant (ε_r) and loss tangent ($\tan\delta$) of BNT-BT-BST ceramics, (a) $x = 0.04$, (b) $x = 0.06$, (c) $x = 0.08$, and (d) $x = 0.1$. (e) Scaling of the dielectric constant close to T_m. The lines are power-law fits using Eq. (2).

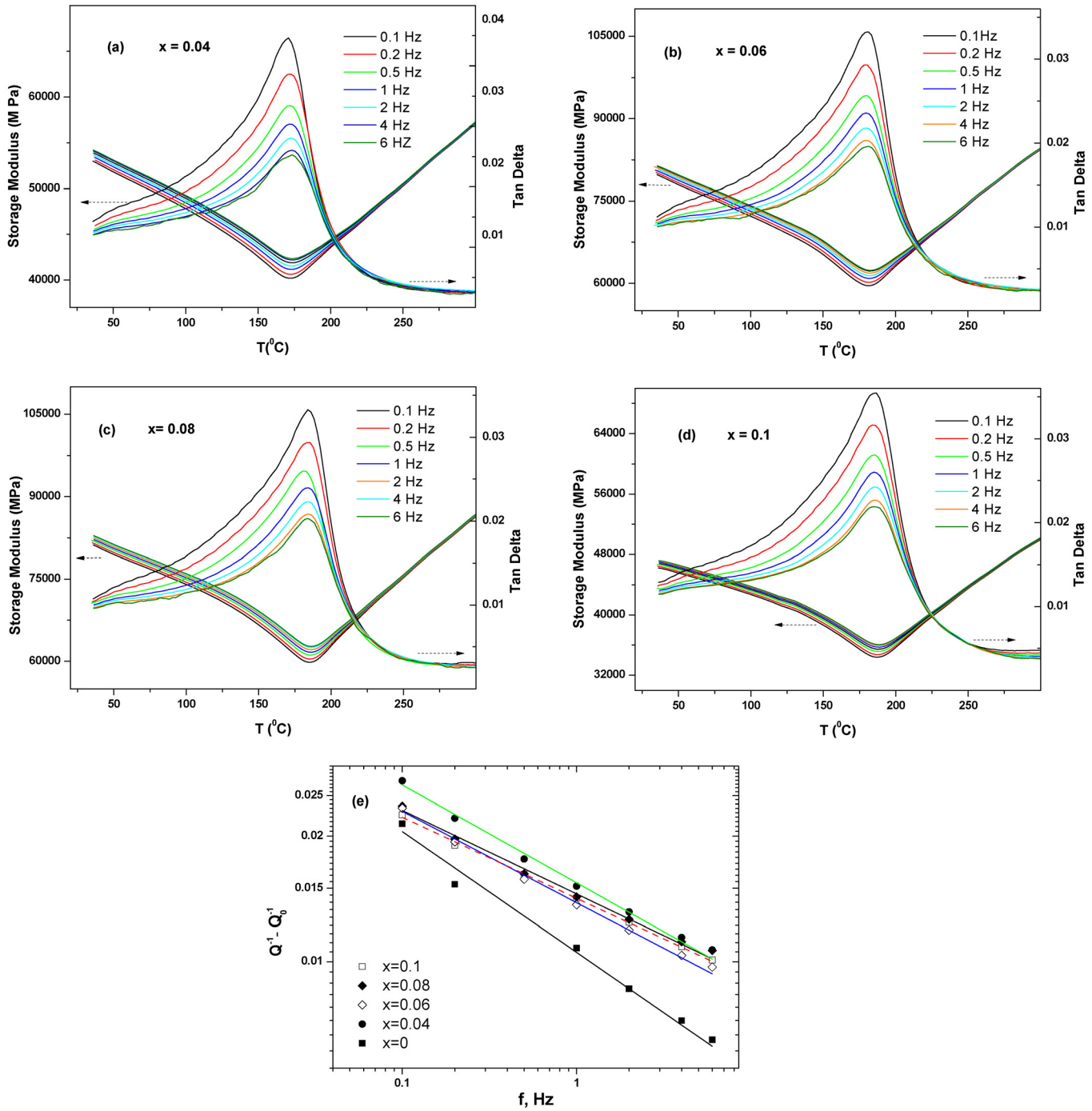

FIG. 7. Frequency and temperature dependence of storage modulus and mechanical loss of BNT-BT-BST ceramics: (a) x = 0.04, (b) x = 0.06, (c) x = 0.08, and (d) x = 0.1. (e) Scaling of the mechanical loss peak height at T_F. The lines are power-law fits using Eq. (3).

could drive the diffuseness of the local domains, leading to the increased local disorder of the dipoles. Therefore, the applied electric field could facilitate the formation of a diffusive PE state, resulting in the negative ECE.

The Curie-Weiss-like relation is used to quantitatively measure the effects of BST doping on the relaxor behavior of BNT-BT-BST

$$\frac{1}{\varepsilon_r} - \frac{1}{\varepsilon_m} \propto (T_m - T)^{\gamma}, \tag{2}$$

where γ is the exponent that characterizes the degree of relaxor behavior, i.e., $\gamma > 1$. ε_m is the maximum dielectric constant at temperature T_m. The scaling for the dielectric constant near T_m using Eq. (2) is shown in Fig. 6(e). The exponent γ is found to first decrease and then increase with increasing BST doping, as shown in Fig. 5(b), demonstrating that the relaxor behavior is stronger in BNT-BT-BST with more BST content ($x > 0.04$), as expected.

In order to verify the effect of BST doping on the structural transformation close to the FE-to-AFE transition temperature, anelastic behavior of the samples was analyzed. The storage modulus and mechanical loss (internal friction) at different frequencies as a function of temperature are shown in Fig. 7. It is quite obvious that the FE-to-AFE phase

transition temperature (T_F) increased with increasing BST content, consistent with the results of the dielectric analyses shown in Fig. 6. The relation between the frequency and internal friction can be used to characterize the dynamics of the interface between FE and AFE domain walls. The peak height relative to the background of the internal friction peak Q^{-1} can be scaled with respect to the frequency f as[22]

$$(Q^{-1} - Q_0^{-1}) \propto f^{-\beta}, \quad (3)$$

where Q_0^{-1} is the frequency-independent internal friction background at the peak temperature. The exponent $0 < \beta < 1$ in Eq. (3) measures the stiffness of the interface between FE and AFE domain walls,[23] e.g., the stiffness of the phase interface increases with decreasing β. The effect of BST doping on the structural transformation related to the FE-to-AFE transition is characterized by using Eq. (3), as shown in Fig. 7(e). The relation between the exponent β and BST doping is shown in Fig. 5(b). Since the exponent β decreases with the increasing BST doping, the stiffness of the phase interface is higher when more BST are doped; hence, BST doping favors the FE state while the applied electric field favors the AFE state. Hence the ECE temperature change $|\Delta T|$ slightly decreases with BST doping, as shown in Fig. 5(b).

In summary, the dielectric and anelastic analyses revealed that the unified (negative) ECE behavior of the BNT-BT-BSTA ceramics could be caused by the convergence of the FE-to-AFE and AFE-to-PE transitions, the stabilization of the FE state at higher temperatures and the enhanced diffuseness of the AFE-to-PE transition with increasing BST content (i.e., $x > 0.06$).

IV. CONCLUSIONS

Solid-solution compounds $(1\text{-}x)(0.94Bi_{1/2}Na_{1/2}TiO_3\text{-}0.06BaTiO_3)\text{-}xBa_{1/2}Sr_{1/2}TiO_3$ ($x = 0.04$, 0.06, 0.08, and 0.1) were fabricated via the sol-gel method. The electrocaloric properties of the fabricated ceramic samples were investigated by using the thermodynamics Maxwell relations. It was observed that ECE depends critically on the phase transition behavior of the ferroelectric materials. The doping of BST into the lattice of 0.94BNT-0.06BT affected the phase transitions of the samples and the FE phase was stabilized at a higher temperature. The ECE of the samples was unified by the doping of BST and the degree of unification was increased by increasing the BST content up to 10 mol. %. The results of this work demonstrate that $(1-x)(0.94Bi_{1/2}Na_{1/2}TiO_3\text{-}0.06BaTiO_3)\text{-}xBa_{1/2}Sr_{1/2}TiO_3$ with a negative ECE can be a promising refrigerants.

ACKNOWLEDGMENTS

This work was supported by the Program for Professor of Special Appointment (Eastern Scholar) at Shanghai Institutions of Higher Learning. The authors acknowledge the financial support by the Higher Education Commission (HEC) of Pakistan under the International Research Support Initiative Program (IRSIP), the Science and Technology Innovation Commission of Shenzhen, China, and the NAS (USA) and HEC (Pakistan) Pakistan-US Science and Technology Cooperative Program (Project ID 131).

[1]P. Kobeco and I. V. Kurtchatov, "Dielectric properties of Rochelle salt crystal," Z. Phys. **66**, 192–205 (1930).
[2]Y. Bai, G. P. Zheng, and S. Q. Shi, "Abnormal electrocaloric effect of $Na_{0.5}Bi_{0.5}TiO_3$–$BaTiO_3$ lead-free ferroelectric ceramics above room temperature," Mater. Res. Bull. **46**, 1866–1869 (2011).
[3]W. N. Lawless, "Specific heat and electrocaloric properties of a $KTaO_3$ at low temperatures," Phys. Rev. B **16**(1), 433–439 (1977).
[4]W. N. Lawless and A. J. Morrow, "Specific heat and electrocaloric properties of a $SrTiO_3$ ceramic at low temperatures," Ferroelectrics **15**, 159–165 (1977).
[5]B. A. Tuttle and D. A. Payne, "The effects of microstructure on the electrocaloric properties of Pb(Zr, Sn, Ti)O_3 ceramics," Ferroelectrics **37**, 603–606 (1981).
[6]B. Nesse, B. Chu, S. G. Lu, Y. Wang, E. Furman, and Q. M. Zhang, "Large electrocaloric effect in ferroelectric polymers near room temperature," Science **321**, 821–823 (2008).
[7]J. Hagberg, A. Uusimaki, and H. Jantunen, "Electrocaloric characteristics in reactive sintered 0.87 $Pb(Mg_{1/3}Nb_{2/3})O_3$–0.13 $PbTiO_3$," Appl. Phys. Lett. **92**, 132909 (2008).
[8]X. C. Zheng, G. P. Zheng, Z. Lin, and Z. Y. Jiang, "Electrocaloric behaviors of BNT-BT ceramics," J. Electroceramics **28**, 20 (2012).
[9]M. Valant, L. J. Dunne, A. K. Axelsson, N. Mc. Alford, G. Manos, and J. Perantie, "Electrocaloric effect in a ferroelectric $Pb(Zn_{1/3}Nb_{2/3})O_3$–$PbTiO_3$ single crystal," Phys. Rev. B **81**, 214110 (2010).
[10]Y. Bai, G. P. Zheng, and S. Q. Shi, "Kinetic electrocaloric effect and giant net cooling of lead-free ferroelectric refrigerants," J. Appl. Phys. **108**, 104102 (2010).
[11]F. L. Goupil, A. Berenov, A. K. Axelsson, M. Valant, and N. M. Alford, "Direct and indirect electrocaloric measurements on 001-$PbMg_{1/3}Nb_{2/3}O_3$-30$PbTiO_3$ single crystals," J. Appl. Phys. **111**, 124109–124116 (2012).
[12]I. Ponomareva and S. Lisenkov, "Bridging the macroscopic and atomistic descriptions of the electrocaloric effect," Phys. Rev. Lett. **108**, 167604–167608 (2012).
[13]A.-K. Axelsson, F. L. Goupil, L. J. Dunne, G. Manos, M. Valant, and N. M. Alford, "Microscopic interpretation of sign reversal in the electrocaloric effect in a ferroelectric $PbMg_{1/3}Nb_{2/3}O_3$-30$PbTiO_3$ single crystal," Appl. Phys. Lett. **102**, 102902–102905 (2013).
[14]M. Xu, F. Wang, T. Wang, X. Chen, Y. Tang, and W. Shi, "Phase diagram and electric properties of the (Mn, K)-modified $Bi_{0.5}Na_{0.5}TiO_3$–$BaTiO_3$ lead-free ceramics," J. Mater. Sci. **46**, 4675–4682 (2011).
[15]F. Wang, M. Xu, T. Wang, Y. Tang, and W. Shi, "Phase transition and electrical properties in the Li-modified $Bi_{0.5}Na_{0.5}TiO_3$-based lead-free ceramics," J. Mater. Sci. **47**, 2352–2358 (2012).
[16]S. T. Zhang, F. Yan, B. Yang, and W. Cao, "Phase diagram and electrostrictive properties of $Bi_{0.5}Na_{0.5}TiO_3$–$BaTiO_3$–$K_{0.5}Na_{0.5}NbO_3$ ceramics," Appl. Phys. Lett. **97**, 122901–122903 (2010).
[17]M. Acosta, J. Zang, W. Jo, and J. Rodel, "High-temperature dielectrics in $CaZrO_3$-modified $Bi_{1/2}Na_{1/2}TiO_3$-based lead-free ceramics," J. Eur. Ceram. Soc. **32**, 4327–4334 (2012).
[18]R. D. Shannon, "Revised effective ionic radii and systematic studies of interatomic distances in halides and chalcogenides," Acta Crystallogr., Sect. A: Cryst. Phys., Diffr., Theor. Gen. Crystallogr. **32**, 751–767 (1976).
[19]G. Trolliard and V. Dorcet, "Reinvestigation of phase transitions in $Na_{0.5}Bi_{0.5}TiO_3$ by TEM. Part II: Second order orthorhombic to tetragonal phase transition," Chem. Mater. **20**, 5074–5082 (2008).
[20]G. O. Jones and P. A. Thomas, "Investigation of the structure and phase transitions in the novel A-site substituted distorted perovskite compound Na0.5Bi0.5TiO3," Acta Crystallogr., Sect. B: Struct. Sci. **58**, 168–178 (2002).
[21]D. Viehland, S. J. Jang, L. E. Cross, and M. Wuttig, "Freezing of the polarization fluctuations in lead magnesium niobate relaxors," J. Appl. Phys. **68**, 2916–2922 (1990).
[22]R. B. Perez-Saez, V. Recarte, M. L. No, and J. San Juan, "Anelastic contributions and transformed volume fraction during thermoelastic martensitic transformations," Phys. Rev. B **57**(10), 5684–5692 (1998).
[23]Y.-N. Wang, X.-H. Chen, and H.-M. Shen, "Recent studies on international friction associated with diffussionless phase transitions and domain walls," in *Proceedings of the ICIFUAS-9*, edited by T. S. Ke (Pergamon, New York, 1990), pp. 305–312.